

Wrapped Composite Joint Additional Graduation Work

Study into linear coefficient of thermal expansion
and modelling of diffusion behaviour in
composites

Janneke Kortsmit



Wrapped Composite Joint Additional Graduation Work

Study into linear coefficient of thermal expansion
and modelling of diffusion behaviour in composites

Additional Graduation Report

by

Janneke Kortsmid

for completion of CIE5050-09 Additional Graduation Work, Research Project
at the Delft University of Technology

Supervisors of project: Dr. M. Pavlovic
Dr. M. Moreira Arouche
ir. M. Wolters
Place: Faculty of Civil Engineering, Delft
Project Duration: September, 2023 - August, 2024
Student number: 4447751

An electronic version of this thesis is available at <http://repository.tudelft.nl/>.



Copyright © Janneke Kortsmid, 2024
All rights reserved.

Abstract

This Additional Graduation Work consists of two different fields of research: experimentally determining the linear coefficient of thermal expansion, and by Finite Element Modelling determining salt water diffusion coefficients. The research is centered around the wrapped composite joint: an innovative technology using a composite wrap connecting steel hollow sections instead of traditional welds.

Linear Coefficient of Thermal Expansion

The Linear Coefficient of Thermal Expansion is determined theoretically and experimentally. The results show for hand layup composites a respectively theoretical and experimental coefficient of $1.85 \cdot 10^{-5}/^{\circ}C$ and $2.15 \cdot 10^{-5}/^{\circ}C$ in longitudinal and transverse direction and of $4.80 \cdot 10^{-5}/^{\circ}C$ and $7.82 \cdot 10^{-5}/^{\circ}C$ in through-thickness direction. For composites produced by a new production method, resulting in a higher fibre volume fraction the respectively theoretical and experimental coefficient is $1.44 \cdot 10^{-5}/^{\circ}C$ and $1.59 \cdot 10^{-5}/^{\circ}C$ in longitudinal and transverse direction and $4.01 \cdot 10^{-5}/^{\circ}C$ and $5.79 \cdot 10^{-5}/^{\circ}C$ in through-thickness direction.

Especially in through-thickness direction difference between theoretical results are up to 62%. This discrepancy is expected to be caused primarily by defects present in the material, as specimens are produced from mechanically tested material. Defects in the material cause discontinuities, which can lead to a higher apparent CTE as the matrix is less confined by fibres.

Diffusion Modelling

With Finite Element Software Abaqus the rate of diffusion of salt water into composite produced by means of hand layup is determined. Experimental results of submersion tests in salt water under room temperature were used for validation of the models. Material is assumed to have a moisture content of 0 at the start of the experiment. On top of that, a saturation of 0.47% is assumed, based on previous research.

Firstly, the in-plane diffusion coefficient $D_{x,y}$ is determined. Results of Finite Element analysis are validated against a slice of non-post cured material with least thickness, and thus primary diffusion direction in longitudinal direction. In Abaqus Fickian behaviour is assumed, with a negligible small diffusion in through-thickness direction. This results in $D_{x,y} = 0.08mm^2/day$.

Secondly, the in-plane diffusion coefficient is used to determine the through-thickness diffusion coefficient by using experimental weight increase by salt water uptake of End Notched Flexure and Interlaminar Shear coupons as validation for Finite Element models. This results in $D_z = 0.03mm^2/day$.

Thirdly, the saturation of a bi-material steel composite End Notched Flexure coupon is numerically determined. It is determined that in 4.6 years the coupon would fully saturate.

The research showed big differences in saturation rates of different geometries and conditions (post cured or non-post cured). This can primarily be explained by the assumption material is dry before experimentally submerging. Especially non-post cured material will have a non-zero begin moisture content. By not taking this into account, the moisture content is underestimated.

Additional experiments including drying of material should be executed to with certainty determine the diffusion coefficient and saturation of the material.

Contents

List of Figures	v
List of Tables	vi
1 Introduction	1
1.1 Coefficient of Thermal Expansion	1
1.2 Diffusion models	1
1.3 Reading guide	1
I Linear Coefficient of Thermal Expansion	2
2 Methodology	3
2.1 Theoretical method	3
2.2 Experimental Methods	4
2.3 Thermomechanical Analysis	6
2.4 Strain gauges	6
2.5 Digital Image Correlation	7
2.6 Selected method to determine Linear Coefficient of Thermal Expansion	8
3 Results	9
3.1 Hand-laminated coefficient of thermal expansion	9
3.2 NM coefficient of thermal expansion	11
4 Discussion and conclusion	12
II Diffusion modelling	14
5 Methodology	15
5.1 Theoretical background	15
5.2 FEA diffusion method	17
5.3 Geometries	18
6 Results	20
6.1 Experimentally determined diffusion coefficients	20
6.2 Prediction diffusion profile bi-material coupons	24
7 Discussion and conclusion	26
References	29

Nomenclature

List of Abbreviations

AGW	Additional Graduation Work
CLT	Classical Laminate Theory
CSM	Chopped Strand Mat
CTE	Coefficient of Thermal Expansion
DIC	Digital Image Correlation
ENF	End Notched Flexure
FEA	Finite Element Analysis
GF	Gauge Factor
HLU	Hand layup
ILS	Inter-laminar shear
LVDT	Linear Variable Differential Transformer
NM	New production Method
TMA	Thermal Mechanical Analysis
UD	Uni-directional

List of Symbols

α	Coefficient of Thermal Expansion
κ_p	Pressure stress factor
κ_s	Temperature gradient factor
J	Flux of concentration
ν	Poissons ratio

ϕ	Normalized concentration
θ	Temperature
θ^Z	Absolute zero temperature
A	Surface area
C	Concentration of particles in a volume
D	Diffusion coefficient
dm	Change of amount of particles
dt	Small time increment
E	Young's Modulus
h	Thickness
J	Flux of particles
M_m	Maximum moisture content/Saturation
p	Equivalent pressure stress
R	Resistance
S	Sum of errors
s	Solubility
T	Temperature
V	Voltage
V_f	Fibre Volume Fraction
x	Position
D	Diffusivity

List of Figures

1.1	Indication of directions of CTE	1
2.1	Drawing of a vitreous silica rod [4]	4
2.2	Example of horizontal push-rod dilatometer [5]	5
2.3	Measurement methods of linear CTE using interferometry [7]	5
2.4	TMA 4000 machine [8]	6
2.5	Wheatstone bridge configuration	6
2.6	Embedding process of sample A.1	8
3.1	HLU linear CTE in directions 1, 2 and 3	10
3.2	NM linear CTE in direction 3	11
5.1	Fickian moisture content change [12]	15
5.2	Hydrolysis of a vinyl ester polymer [14]	16
5.3	Schematic representation of long-term diffusion contribution [15]	16
5.4	Experimental coupon dimensions in mm	18
5.5	Bi-material ENF coupon	19
6.1	ENF slice moisture content graphs	20
6.2	FEA results alongside average experimental results ENF slice	21
6.3	FEA results alongside average experimental results post cured ILS coupon	22
6.4	FEA results alongside average experimental results composite ENF coupon	23
6.5	Sections used for saturation profiles	24
6.6	Salt water concentration section B-B	24
6.7	Salt water concentration section A-A. Blue bar = steel plate	25
7.1	Experimental ILS coupon with sketched diffusion curves. Black = Fickian diffusion, blue = additional diffusion due to degradation	27

List of Tables

2.1	Material properties of vinyl ester resin and glass-fibre [2]	3
2.2	Calculated CTE for UD ply and woven-CSM ply	4
3.1	Linear CTE per direction	9
3.2	Linear CTE per direction, where direction 1 and 2 are calculated	11
4.1	Linear CTE	12
6.1	Determined first estimations Diffusion coefficients D_x	20
6.2	ENF slice sum of errors for different diffusion coefficients	21
6.3	ILS sum of errors for different diffusion coefficients	22
6.4	ILS sum of errors first stage for different diffusion coefficients	22
6.5	Composite ENF coupon sum of errors for different diffusion coefficients	23
6.6	Diffusion coefficients	23

1

Introduction

This Additional Graduation Work (AGW) is centered around the wrapped composite joint: an innovative technology aiming to help accelerate the offshore wind industry. Offshore foundation structures are currently based on steel members and welded joints. The steel welds result in heavy structures that are prone to fatigue and cracking in the weld due to local stress concentrations. The wrapped composite joint is a composite wrap designed to prevent the use of welded complex joints. It combines a larger contact surface over which to distribute loading between the chord and brace with an optimal shape, decreasing stress concentrations [1]. This results in longer fatigue life compared to a traditional welded joint.

However, in offshore conditions, the composite material is subjected to harsh environmental conditions. To be able to predict the impact of these factors, research into effects of exposure to salt water and exposure to freeze-thaw cycles is being conducted by TU Delft and Tree Composites. This AGW contributes by tackling two specific subjects; the linear coefficient of thermal expansion (CTE) of the composite and refining of existing salt water diffusion models. All research is conducted on composite consisting of glass fibres with a modified vinyl ester matrix. The fibre plies are of a bi-directional woven fabric stitched to a chopped strand mat (CSM). The composites are either produced by hand layup (HLU) and/or with a new production method (NM). This new production method allows for automation during production, and a higher fibre volume fraction. The following sections discuss per subject the objective and scope. Afterwards a reading guide is added.

1.1. Coefficient of Thermal Expansion

In offshore condition, the composite is subjected to different temperatures. To predict behaviour of the structure, it should be known how much the material expands and contracts. Knowing the CTE gives the possibility to model thermal strains in, for example, the bonded interface between the composite and steel adding valuable insights into the joint behaviour.

This research consists of measuring the linear CTE in three directions; through-thickness (3) and in both in-plane directions, longitudinal (1) and transverse (2) as shown in Figure 1.1 for HLU and NM composites.

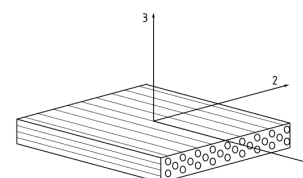


Figure 1.1: Indication of directions of CTE

1.2. Diffusion models

In ongoing research HLU composite and steel-composite specimens of different geometry are submerged in salt water. The weight change of these specimens is measured to gain understanding on the diffusivity of salt water into the composite material. These measurements are used to predict the moisture diffusion using Finite Element Analysis (FEA) software Abaqus. For this AGW these models will be further improved. This improved model is then used to determine the saturation profile for other geometries.

The goal is to model the diffusion and determine the diffusion coefficients of HLU material in different directions.

1.3. Reading guide

The report is divided into two parts. Part I discusses the linear CTE and Part II the diffusion models. Both parts are divided in method, results, discussion and conclusion. Due to the different nature of the two experiments, there will be no general conclusion and discussion combining both parts.

Part I

Linear Coefficient of Thermal Expansion

2

Methodology

This chapter describes different methods that can be used to determine the linear CTE of a fibre reinforced composite. First, a theoretical method for calculating the CTE is applied. Afterwards, different experimental methods are summarised with advantages and limitations. To conclude Section 2.6 describes the used method.

2.1. Theoretical method

To calculate the theoretical linear CTE, Appendix B of prCEN/TS 19101 [2] is used in combination with software *eLamX²*. The software is a composite calculator using classical laminate theory (CLT) [3].

Table 2.1 summarises material properties as shown in prCEN/TS 19101 [2]. The lower bound represents the lowest indicative value and the higher bound the highest indicative value. However, as these values are determined from literature, they do not represent experimentally determined properties of the modified vinyl ester resin or glass fibre used in this research. α represents the CTE in 1- and 2-direction, as defined in Figure 1.1.

Table 2.1: Material properties of vinyl ester resin and glass-fibre [2]

	Vinyl ester		Glass fibre
	Lower bound	Upper bound	
E_1, E_2 [GPa]	3.3	3.5	74
Poissons ratio (ν) [-]	0.38	0.38	0.25
α_1, α_2 [$\cdot 10^{-6} \text{ }^\circ\text{C}^{-1}$]	30	50	5

The material properties as shown in Table 2.1 can be used to calculate properties of a uni-directional (UD) ply. These ply properties can be calculated by using the following formulas [2]

$$E_1 = E_r + (E_{f,1} - E_r) \cdot V_f \quad (2.1)$$

$$E_2 = \frac{E_f \cdot E_m}{V_f \cdot E_m + V_m \cdot E_f} \quad (2.2)$$

$$\nu_{12} = \nu_r - (\nu_r - \nu_f) \cdot V_f \quad (2.3)$$

$$\frac{\nu_{12}^{UD}}{E_1^{UD}} = \frac{\nu_{21}^{UD}}{E_2^{UD}} \quad (2.4)$$

$$\alpha_1 = \frac{V_f \cdot \alpha_{f,1} + V_r \cdot \alpha_r \cdot E_r}{E_1} \quad (2.5)$$

$$\alpha_2 = (1 + \nu_f) \cdot \alpha_{f,2} \cdot V_f + (1 + \nu_r) \cdot \alpha_r \cdot V_r - \alpha_1 \cdot \nu_{12} \quad (2.6)$$

Where

- E_1, E_2 = in-plane elastic modulus of ply in direction 1 and 2
 E_r = elastic modulus of resin
 $E_{f,1}, E_{f,2}$ = elastic modulus of fibre in direction 1 and 2
 V_f = fibre volume fraction
 ν_{12} = Poisson's ratio of the ply
 ν_r = Poisson's ratio of the resin
 ν_f = Poisson's ratio of the fibre

However, the ply is not UD, but consists of a bi-directional woven fabric stitched to a CSM. *eLamX²* is used as tool to estimate E_1 and E_2 for this combined ply. The woven fabric is represented by two layers of 0° and 90° fibre direction. The CSM is represented by a set of 18 layers, which all have a angle offset of 5° to each other. The thickness of the woven fabric and CSM layer is based on the relative contribution to the weight of a combined ply. The in total 20 layers form 1 ply. This ply is then symmetrically represented. Table 2.2 shows the CTE of a UD ply, and the CTE of a bi-directional woven stitched CSM ply in longitudinal (1) and transverse (2) direction.

Table 2.2: Calculated CTE for UD ply and woven-CSM ply

	HLU		NM	
	lower bound	upper bound	lower bound	upper bound
$\alpha_1^{UD} [\cdot 10^{-5} \text{ } ^\circ\text{C}^{-1}]$	0.76	0.99	0.65	0.78
$\alpha_2^{UD} [\cdot 10^{-5} \text{ } ^\circ\text{C}^{-1}]$	2.90	4.80	2.45	4.01
$\alpha_1 [\cdot 10^{-5} \text{ } ^\circ\text{C}^{-1}]$	1.23	1.90	1.01	1.45
$\alpha_2 [\cdot 10^{-5} \text{ } ^\circ\text{C}^{-1}]$	1.23	1.90	1.01	1.45

2.2. Experimental Methods

This section describes the methods available to measure the CTE of a material. Each method will be briefly introduced, with advantages and limitations, to help guide in the decision of the definitive used method.

2.2.1. Vitreous Silica Dilatometer

ASTM D696-16 describes a test method for determining the CTE of plastics between -30°C and 30°C [4], by use of a vitreous silica dilatometer, shown in Figure 2.1. The complete rod is immersed in a temperature controlled environment. A dial gauge, linear variable differential transformer (LVDT) or similar device is used to track the displacements. The silica tube and rod both have a very low CTE. By indirectly measuring displacement, the expansion of the set-up is disconnected from the expansion of the material.

Advantages and limitations that should be considered are as follows

- + Specimen preparation and testing is relatively easy
- + Suitable for random and continuous fibres
- Limited to temperature range of -30°C and 30°C
- Material should have CTE greater than $1 \cdot 10^{-6} / ^\circ\text{C}^{-1}$.

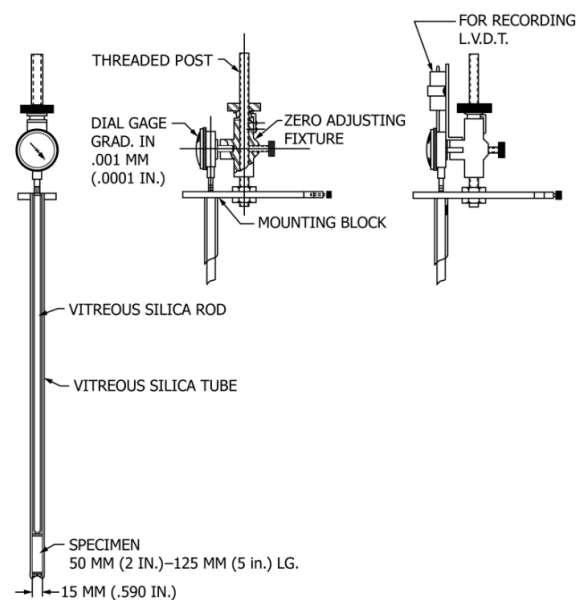


Figure 2.1: Drawing of a vitreous silica rod [4]

2.2.2. Push-rod Dilatometer

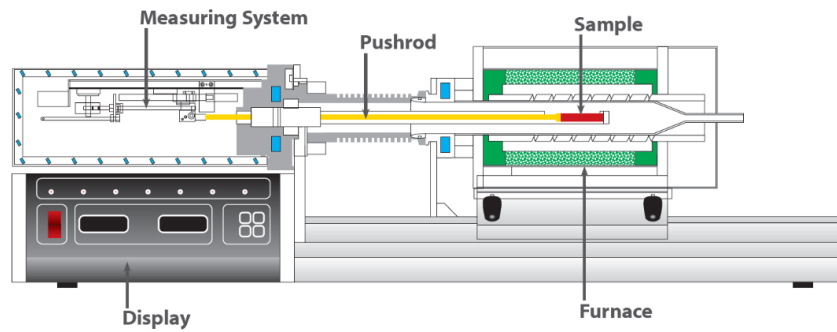


Figure 2.2: Example of horizontal push-rod dilatometer [5]

Similar to the Vitreous Silica Dilatometer, is the measuring of the CTE with a Push-rod Dilatometer as shown in Figure 2.2. The main difference is the sample pushes directly against the push-rod when expanding. This movement is then directly measured by a connected LVDT or strain gauge. Therefore, the measured values are relative values, as they include the expansion of the rod, exposed to the same temperature conditions as the sample. ASTM E228-22 [6] describes a test method for determining the CTE of solid materials with a push-rod dilatometer.

Advantages and limitations that should be considered are as follows

- + Suitable for (dis)continuous fibre composites with defined orientation
- + Suitable for low values of thermal expansion
- + Greater precision than Vitreous Silica Dilatometer
- + Temperature range between $-180\text{ }^{\circ}\text{C}$ and $900\text{ }^{\circ}\text{C}$
- Precision lower than measurement by interferometry

2.2.3. Interferometry

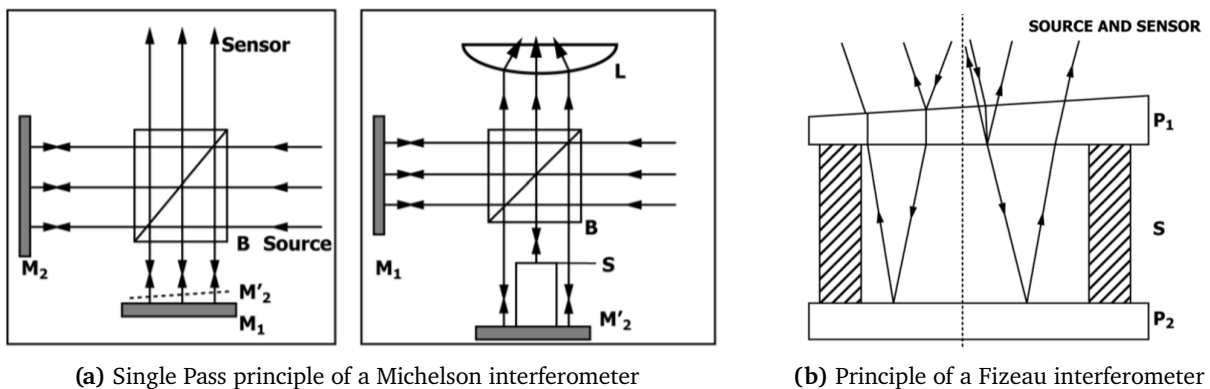


Figure 2.3: Measurement methods of linear CTE using interferometry [7]

This method involves the change of an incoming light signal using parallel light beams and is described in, for example ASTM-E289 [7]. In general two types of interferometers can be used

- Michelson interferometer (Figure 2.3a)
- Fizeau interferometer (Figure 2.3b)

Both principles rest on the direction of the incoming light-beam altering when the to be tested specimen expands or contracts due to temperature changes. These changes in incoming light-beam can be translated into the deformations. With the original length and the temperature change, the CTE can then be calculated.

Both methods require a very precise set-up of all mirrors and sensors in play. When measurements are not undertaken in vacuum or low pressure helium, the surrounding air can result in optical drifts and inaccuracies of measurements. Next to that, the environment should be vibration-less to prevent inaccuracies. To adequately heat and cool a specimen during testing the complete set-up should be placed in a furnace. The advantages and limitations of this method are as follows

- + Temperature range between $-150\text{ }^{\circ}\text{C}$ to $150\text{ }^{\circ}\text{C}$
- + Precision greater than $\pm 40 \cdot 10^{-9}\text{ }^{\circ}\text{C}^{-1}$
- + Suitable for material with very low linear CTE
 - Complicated set-up
 - Complicated specimen preparation

2.3. Thermomechanical Analysis

The thermomechanical analysis (TMA) can be used to determine the CTE, according to ISO 11359-2 [9]. The method requires a machine like shown in Figure 2.4. The sample is housed in a holder with a low CTE. An expansion probe applies a compressive force on the specimen, keeping it in place, and registering displacements via an indirect connected LVDT as temperature changes. The furnace controls the temperature of the sample and changes temperature with a constant rate of maximum $5\text{ }^{\circ}\text{C}/\text{min}$.

The most relevant advantages and limitation are:

- + Specimen preparation relatively easy
- + Ease of testing
 - Material should have CTE great than $1 \cdot 10^{-6}\text{ }^{\circ}\text{C}^{-1}$

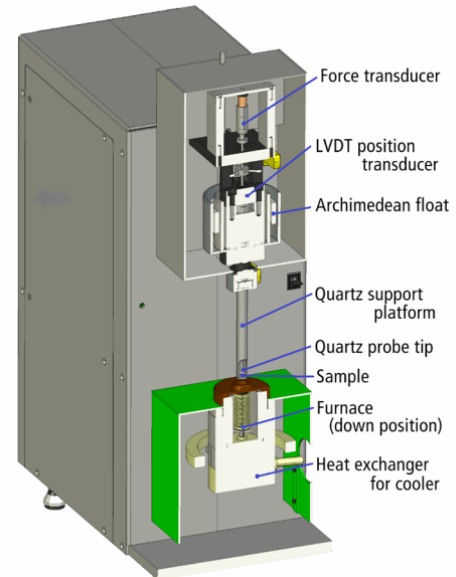


Figure 2.4: TMA 4000 machine [8]

2.4. Strain gauges

A method not described in standards that could be used to determine the CTE, is by using strain gauges. By using a Wheatstone bridge configuration connected to the sample and a reference sample with known CTE, both subjected to the same temperature, the thermal strains can directly be determined whilst taking into account the thermal strains developing in the gauges themselves. Figure 2.5 shows the configuration of the resistors. Any combination of two resistors can be switched for strain gauges.

If assuming R_1 and R_3 are the strain gauges, when there is strain in the specimen, the output voltage and input voltage will not be equal.

$$V_{OUT} = \frac{V_{IN}}{2} \cdot \left(\frac{\Delta R_1}{R_1} - \frac{\Delta R_3}{R_3} \right) \quad (2.7)$$

$$\Delta R_i = R_i \cdot GF \cdot \alpha_i \cdot \Delta T \quad (2.8)$$

$$\alpha = \frac{2 \cdot V_{OUT}}{V_{EX} \cdot GF \cdot \Delta T} + \alpha_{ref} \quad (2.9)$$

$$\alpha_x = \alpha_r + \frac{\epsilon_{xa} - \epsilon_r}{\Delta T} \quad (2.10)$$

Where

V_{out} = Voltage measured over the bridge

V_{in} = input voltage

ΔR_i = the resistance change due to change in strain

ΔT = change in temperature

GF = gauge factor; change in electrical resistance when exposed by mechanical strain

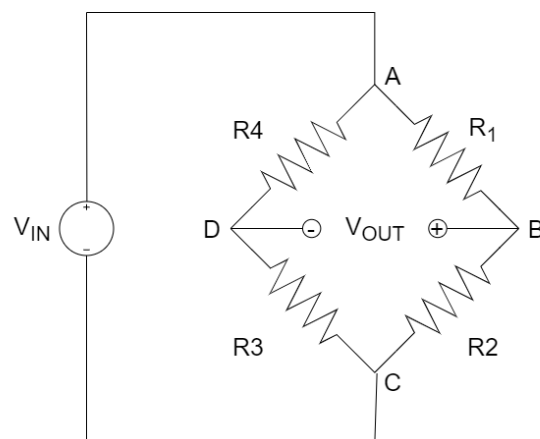


Figure 2.5: Wheatstone bridge configuration

However, there are still numerous challenges that should be considered with this method, summarised in these advantages and limitations

- + Simple sample preparation
- Strain gauges should be of the same production batch, to prevent differences in expansion of the strain gauges themselves
- Placement of the strain gauges should be very precise to avoid errors due to misalignment
- When the sample heats up, it can further heat up the strain gauges, causing apparent strain measurements

2.5. Digital Image Correlation

Another method for determining the CTE is using Digital Image Correlation (DIC). Simply put, the method consists of applying white paint with a random black speckle pattern on a sample. A camera will then track the movement of individual speckles. This gives the possibility to track strains in a material. A division can be made for two measuring methods using a DIC-system:

1. Active change of temperature by use of a temperature controller
2. Passive change of temperature by letting a sample cool down/heat up to ambient temperatures

The following sub-sections will discuss experimental set-ups that could be used, with the advantages and limitations of the specific method.

2.5.1. Active temperature control

This method involves having a sample in a controlled temperature environment whilst registering deformations. To prevent inaccuracies when measuring, the camera cannot be a part of this controlled environment. The result is an enclosed environment with a glass surface through which the camera can track the speckles. Using an enclosed environment with glass and using DIC introduces multiple challenges. This can be summarised in the following advantages and limitations:

- + There is no direct contact between sample and set-up, so there is less disturbance of the sample compared to, for example with the use of a dilatometer
- + Environmental conditions are of high accuracy and highly controllable
- The sample should be able to freely expand and contract to obtain an accurate CTE measurement. However, due to the changing temperature rigid body rotations will take place, which have to be compensated in the measurements to get accurate results, complicating post-processing
- Attention should be paid on the glass surface, as it will cause refraction of the light. To accurately track the speckles, this should be compensated for in post-processing
- The glass should be of a lowest possible CTE itself, to prevent even further change of refraction of light due to deformations
- When heating samples in a non-enclosed environment, sufficiently small samples should be used to prevent uneven heating throughout the sample.

2.5.2. Passive temperature control

This method involves heating or cooling down a specimen in a furnace or freezer. After it reaches the desired temperature, it is taken out, placed on the measuring surface. The temperature change towards ambient temperature is then registered with the DIC-system.

- + Experimental set-up is relatively easy
- No control of speed of heating and cooling of a sample can cause a non-uniform temperature distribution through the sample, which can result in measuring inaccuracies
- As with active temperature control, the rigid body displacements of the sample will need to be compensated for

2.6. Selected method to determine Linear Coefficient of Thermal Expansion

Due to equipment availability and ease of use, a TMA instrument as described in Section 2.3 is used. This section describes the machine, used materials and sample preparation and how the data will be post-processed.

2.6.1. Equipment

For the experiment a PerkinElmer TMA 4000 as shown in Figure 2.4 is used. The sample is heated up with a speed of 2 °C/min from -30 °C to 60 °C. To keep the specimen in place, a downward compressive force of 0.5N is applied. Heating rate and compressive force are based on experience of lab technicians of the Faculty of Aerospace Engineering of TU Delft. The machine registers the displacement of the sample and the temperature with a thermocouple positioned in the quartz support platform near the sample. A sample has a maximum height of 7.5mm, a maximum diameter of 8.5mm and should have parallel surfaces. The sample height is measured with a caliper before starting of the experiment.

2.6.2. Used materials

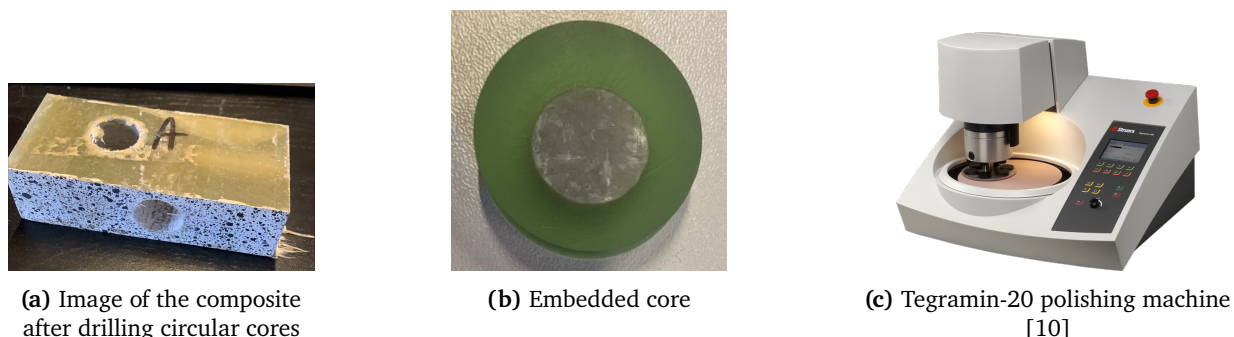


Figure 2.6: Embedding process of sample A.1

For the tests HLU and NM composite specimens are used. Out of larger composite samples manufactured for mechanical tests, circular cores are drilled using a drill press and a plug drill bit in length-wise (1), transverse (2) and thickness (3) direction, resulting in a sample like in Figure 2.6a.

Firstly, the sample preparation method is tested. A HLU specimen was drilled through the thickness using a 10mm plug steel drill bit. The sample is then cut into 11mm thick slices. One slice was embedded in a cold-curing resin (Figure 2.6b) to be able to afterwards use an Tegramin-20 semi-automatic polishing machine (Figure 2.6c) to reduce the thickness of the sample and ensure it has parallel surfaces. After preparation, a 8mm plug drill was used to drill the definitive sample out, making sure no embedding resin remains part of the sample. However, the preparation method was deemed unsuitable. The embedding resin cures at temperatures above the glass transition temperature of the used material, thus introducing a thermal cycle, which could affect the CTE. In addition, it showed to be a very labour intensive method.

For all following samples, 8mm drilled cores were manually sanded to be as parallel as possible. In total 3 HLU and NM samples were produced in through-thickness (3) direction. On top of that 2 transverse (2) and 3 longitudinal (1) HLU samples were produced. Directions are as indicated in Figure 1.1 Due to insufficient thickness of NM material, it was impossible to produce specimens in in-plane directions.

2.6.3. Post-processing

The TMA 4000 as results gives temperature and displacement values relative to the begin height. A figure is plotted with temperature on the x-axis and strain on the y-axis. The strain is calculated by dividing the displacement by the initial length. To find the CTE, the linear trend line fitting the experimental data is plotted. The slope of this line then represents the CTE. To prevent taking along initial fluctuations in measurements, the range of -25 °C to 60 °C is taken into account for the trend line.

3

Results

This section describes the results obtained from the TMA of the material. They are split in HLU and NM in different directions. As defined in Figure 1.1, direction 1 represents the in-plane direction with slightly more fibres present than perpendicular to this plane: direction 2. through-thickness is represented as direction 3.

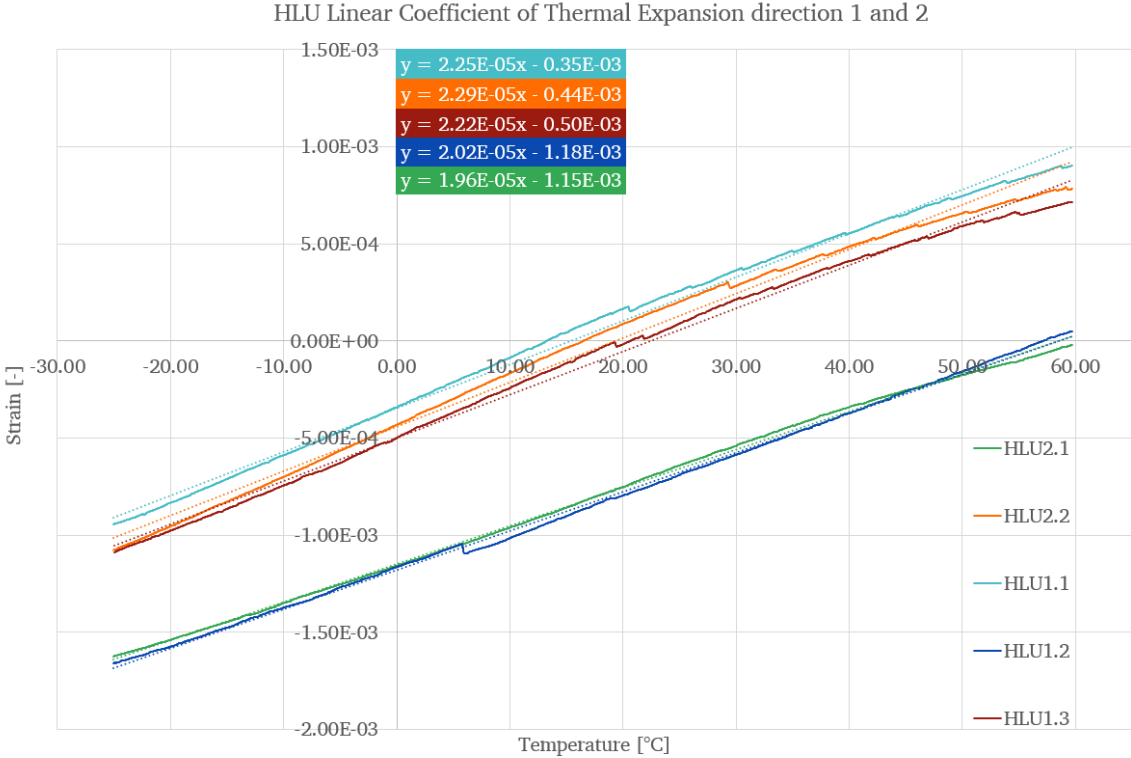
3.1. Hand-laminated coefficient of thermal expansion

Figure 3.1 shows the thermal strains versus temperature in directions, 1, 2 and 3. The direction of the trend line represents the linear CTE of that specific sample, also summarised in Table 3.1.

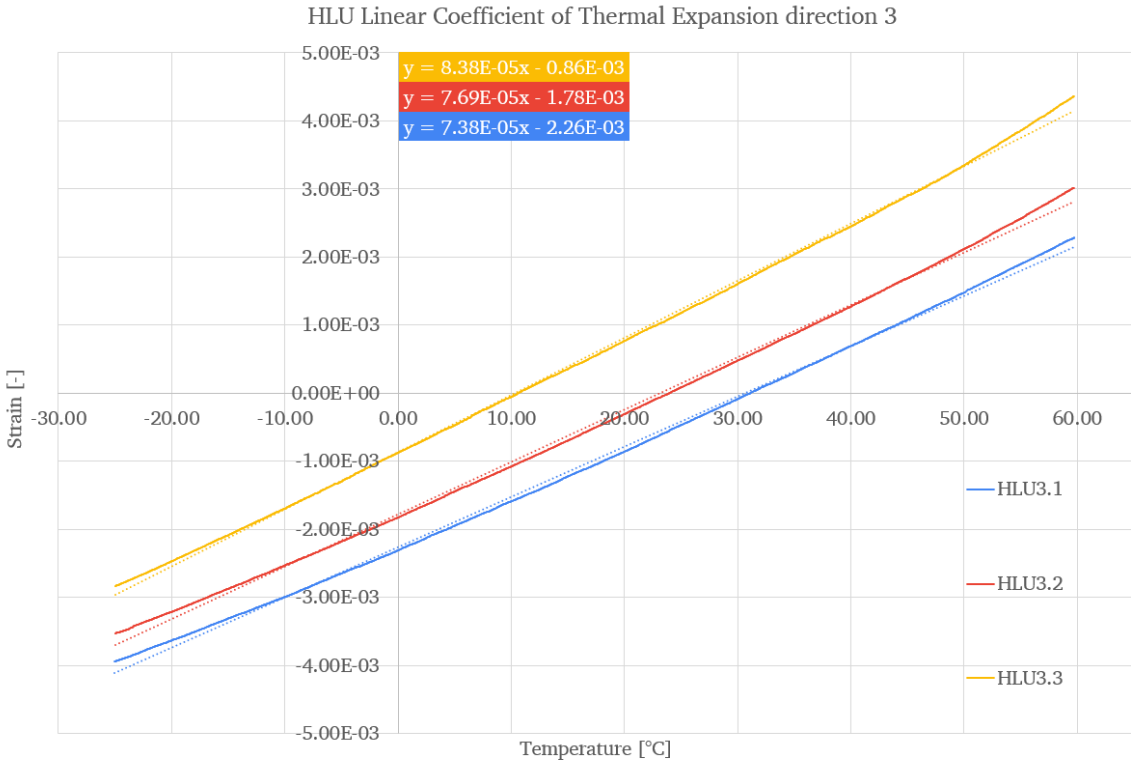
Table 3.1: Linear CTE per direction

Direction	#	CTE [$10^{-5}/^{\circ}\text{C}$]	Average [$10^{-5}/^{\circ}\text{C}$]	Standard Deviation [$\cdot 10^{-5}$]
1	1	2.25	2.16	0.125
1	2	2.02		
1	3	2.22		
2	1	1.96	2.13	0.233
2	2	2.29		
3	1	7.38	7.82	0.512
3	2	7.68		
3	3	8.38		

Figure 3.1 shows jumps in all in-plane measurements. This can be explained due to the challenges with producing in-plane sample. By drilling a core in direction of fibres, the fibres can let loose, leaving an uneven surface. This can cause additional movement of the sample during testing, causing the sudden jump in displacement measurement.



(a) Direction 1 and 2



(b) Direction 3

Figure 3.1: HLU linear CTE in directions 1, 2 and 3

3.2. NM coefficient of thermal expansion

Figure 3.2 shows the thermal strains versus temperature in direction 3. The slope of the trend line represents the linear CTE of that specific sample. This is also summarised in Table 3.2. To estimate the NM in-plane linear CTE, the same ratio between in-plane and through-thickness CTE is applied as visible in the HLU results, summarised in Table 3.1.

Table 3.2: Linear CTE per direction, where direction 1 and 2 are calculated

Direction	#	CTE [$10^{-5}/^{\circ}\text{C}$]	Average [$10^{-5}/^{\circ}\text{C}$]	Standard Deviation [$\cdot 10^{-6}$]
1	-	-	1.60	-
2	-	-	1.57	-
3	1	5.82	5.79	1.12
3	2	5.89		
3	3	5.67		

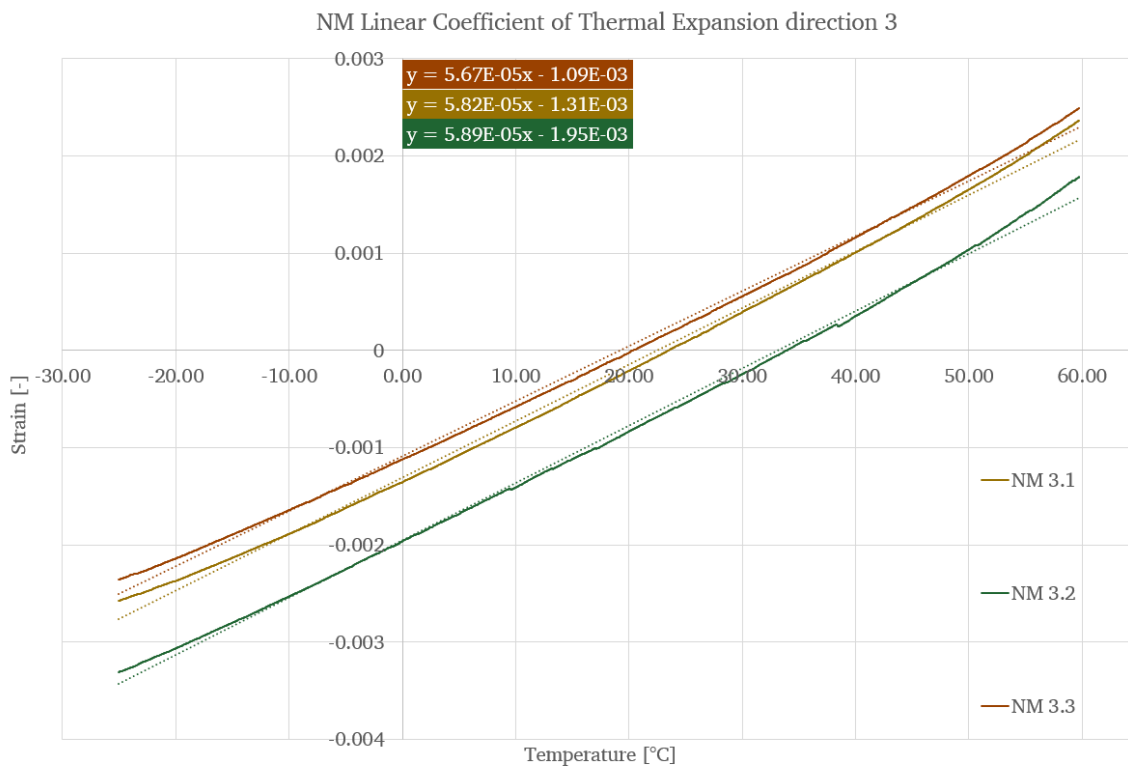


Figure 3.2: NM linear CTE in direction 3

4

Discussion and conclusion

Table 4.1 summarises the experimentally (Chapter 3) and theoretically (Section 2.1) determined CTE for HLU and NM composites. The through-thickness (3) direction contains no load-bearing fibres, similar to the transverse (2) direction of a UD ply. The theoretical CTE is thus assumed to be equal, and included in Table 2.2.

Table 4.1: Linear CTE

Direction	Production method	Experimental CTE [$10^{-5}/^{\circ}\text{C}$]	Theoretical CTE [$10^{-5}/^{\circ}\text{C}$]
1,2	HLU	2.15	1.23 - 1.85
3	HLU	7.82	2.90 - 4.80
1,2	NM	1.59	1.00 - 1.44
3	NM	5.79	2.45 - 4.01

When considering the results shown in Table 3.1, Table 3.2 and Table 4.1, some points can be commented on:

- A mean deviation in the experimental results of less than 10% is registered, which is deemed acceptable due to the non-homogeneous nature of the composite material.
- The fibre volume fractions used in the calculations are based on burn-off tests conducted on thin plates. Thin plates are easier to produce, and therefore could have reached higher fibre volume fractions, by, for example, more efficiently squeezing out excess resin. The used fibre volume fractions could therefore be an overestimation. A higher matrix volume fraction would directly lead to a higher theoretical and experimental CTE, as the CTE of the matrix is almost 10 times higher, as seen in Table 2.1.
- The theoretical CTE is calculated with material properties from literature, not measured properties of the used materials. A higher CTE for the fibre or matrix would directly increase the theoretical CTE. To get a more accurate estimation, material properties of the components should be investigated on.
- In all experiments, mechanically tested material is used. This will result in the material containing defects, such as micro-cracks. These defects result in a discontinuity in the material, which can lead to a higher apparent CTE. When the material is whole, fibres, with lower CTE, will prevent the matrix from expanding. If the material is not whole, this effect will be less, resulting in a higher apparent CTE. In through-thickness direction this effect will be the biggest, as plies can be fully separated in this direction. This can result in multiple layers of almost loose material.
- Experimentally in-plane CTE is shown to be higher than theoretical values:
 - HLU CTE of $2.15 \cdot 10^{-5} \text{ }^{\circ}\text{C}^{-1}$ is 16% above the theoretical upper bound value of $1.85 \cdot 10^{-5} \text{ }^{\circ}\text{C}^{-1}$.
 - NM CTE of $1.59 \cdot 10^{-5} \text{ }^{\circ}\text{C}^{-1}$ is 10% above the theoretical upper bound value of $1.44 \cdot 10^{-5} \text{ }^{\circ}\text{C}^{-1}$.
 - The in-plane NM CTE is expected to be lower when experimentally determined. As seen in Table 2.1 the resin matrix content is primarily causing a higher CTE, having a range between $3 \cdot 10^{-5} \text{ }^{\circ}\text{C}^{-1}$ - $5 \cdot 10^{-5} \text{ }^{\circ}\text{C}^{-1}$. NM specimens have relatively less resin in the through-thickness direction than in HLU material, which would lead to a greater ratio between in-plane and through-thickness CTE and thus a lower CTE than $1.59 \cdot 10^{-5} \text{ }^{\circ}\text{C}^{-1}$.

- The difference between the experimentally determined CTE of the HLU composite in direction 1 and 2 is minimal. This can be explained by the fibre density being almost equal in both directions. It shows that longitudinal and transverse CTE can be considered one value, not subdivided.
- In through-thickness direction the theoretical values are lower than experimentally determined.
 - HLU CTE of $7.82 \cdot 10^{-5} \text{ }^{\circ}\text{C}^{-1}$ is 62% above the theoretical upper bound CTE of $4.80 \cdot 10^{-5} \text{ }^{\circ}\text{C}^{-1}$
 - HLU ratio between in-plane and through-thickness CTE is about 3.6, at the higher limit of the theoretically calculated ratio between 2.4 and 4.0.
 - NM CTE of $5.79 \cdot 10^{-5} \text{ }^{\circ}\text{C}^{-1}$ is 44% above the theoretical upper bound CTE of $4.01 \cdot 10^{-5} \text{ }^{\circ}\text{C}^{-1}$
 - As mentioned previously, it is expected this large difference is mainly due to the use of mechanically tested material. Next to this, the overestimation of fibre volume fraction and use of literature material properties also can contribute to this, but it is commented these contributions would only cause small changes in the CTE.

The CTE as determined in this research is deemed to be of sufficient accuracy to use in the future development of the wrapped composite joint. It should however be mentioned, that in case essential constituents change, such as resin, fibre and fibre orientation, these values will not be applicable anymore. To increase the certainty of correctness of values, an additional step could be to test virgin, untested material, to make sure that defects that are present, are purely manufacturing defects.

Part II

Diffusion modelling

5

Methodology

This chapter will discuss the methods used to predict the diffusivity of salt water into composite material. First an introduction is given into the theoretical background. Next the method used to model the diffusivity in Abaqus is described in Section 5.2. Closing off, the analysed geometries are summarised.

5.1. Theoretical background

Different theoretical models can be used to describe the flux of particles in a material. The method considered in this research are Fick's laws, and will be explained in this section. Fick's first law can in 1D be expressed as [11]:

$$J = \frac{dm}{dtA} = -D \cdot \frac{\partial C}{\partial x} \quad (5.1)$$

Where

- J = flux of any particles (for example ions) [mol/m^2s]
- dm = the change of amount of particles [mol]
- dt = small increment of time [$seconds$]
- A = surface area of the 1D surface [m^2]
- D = diffusion coefficient [m^2/s]
- C = concentration of particles in the volume [mol/m^3]
- x = position [m]

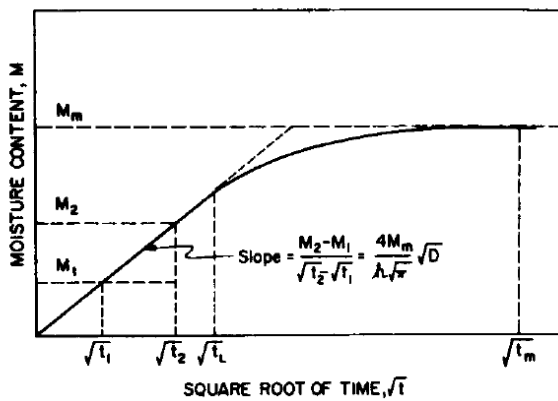


Figure 5.1: Fickian moisture content change [12]

In words, the equation represents the migration of particles from locations of a high concentration to locations of a low concentration. As visible in the equation, the assumption is that only concentration gradient is driving the diffusion, and for example not an externally applied force [11].

This flux of particles will remain constant until the material the diffusion takes place in, reaches its saturation, or maximum moisture content M_m . This is visualized by Figure 5.1, showing the weight increase M [%] versus the square root of time in hours [\sqrt{hours}]. The figure also shows that from the linear part of an experimental diffusion curve, the diffusion coefficient D can be calculated as follows [12]

$$D = \pi \left(\frac{h}{4 \cdot M_m} \right)^2 \left(\frac{M_2 - M_1}{\sqrt{t_2} - \sqrt{t_1}} \right)^2 = \pi \left(\frac{h}{4 \cdot M_m} \right)^2 \cdot slope^2 \quad (5.2)$$

Where

h = thickness of material

M_m = maximum moisture content of material

Equation 5.2 assumes diffusion in only one direction. This assumption is valid when edge effects are minimised, either by minimising the diffusion distance in the direction of interest, or by closing off the sides with coating or other diffusion preventing methods. On top of that a constant temperature and pressure is assumed.

Diffusivity of salt water will follow the curve shown in Figure 5.1 in the first stages. After initial moisture ingress, degradation can cause reversible and irreversible damage, changing the diffusion rate and maximum moisture content. Post curing of material will increase polymerisation and decrease ageing effects.

Plasticisation and swelling are examples of reversible damage. Plasticisation is the phenomena where penetrated water acts as a plasticiser, increasing flexibility of the matrix and softening it. Swelling of the matrix pushes the polymer chains apart, increasing volume and weakening bond between fibre and matrix. In short-term these mechanisms are reversible by drying the material [13].

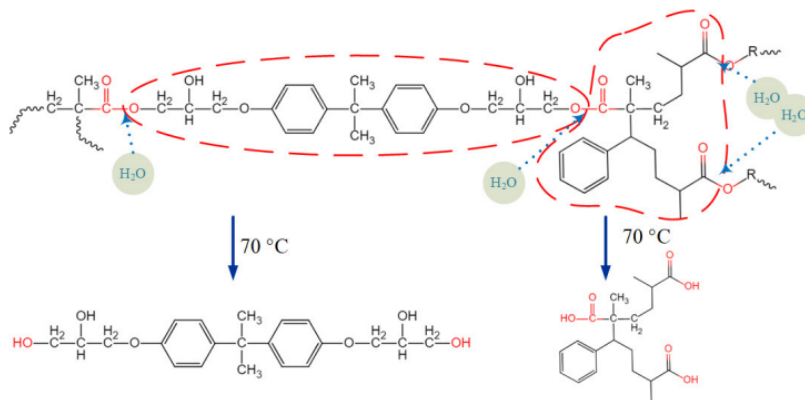


Figure 5.2: Hydrolysis of a vinyl ester polymer [14]

Hydrolysis, micro-cracking and polymer relaxation are irreversible degradation mechanisms. Hydrolysis is the reaction of water molecules with the polymer chain, as shown in Figure 5.2. This reaction 'cuts' the polymer into smaller parts, forming voids, micro-cracks and causing mass loss, reducing strength of the material [14].

Polymer relaxation takes place as polymer chains over longer term move to a new equilibrium state. This reduces internal stresses developed by the diffusion of water. The new equilibrium state will result in redistribution of voids, where more water can enter. This will cause an increase in the maximum moisture content of the material compared to Fickian diffusion as shown in Figure 5.1 [16].

All the above mentioned degradation mechanisms and more, can result in behaviour of the composite being represented by non-Fickian curves. This will either result in weight loss due to leeching of components, or an additional long-term moisture absorption above Fickian behaviour caused by for example polymer relaxation [16]. An example of long-term moisture uptake is shown in Figure 5.3 [15].

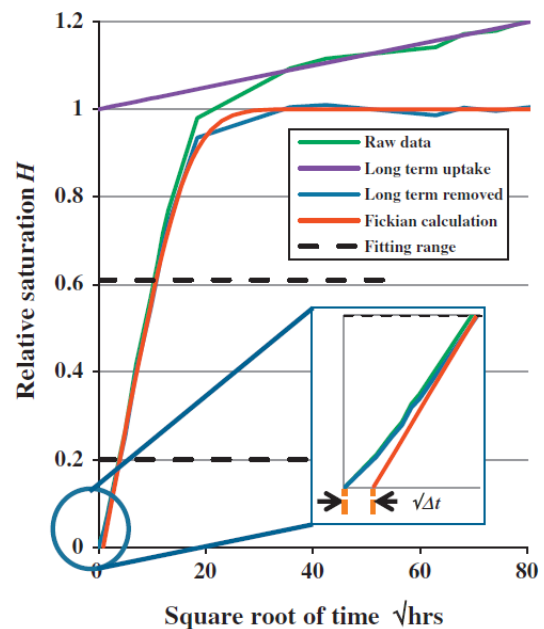


Figure 5.3: Schematic representation of long-term diffusion contribution [15]

5.2. FEA diffusion method

In Abaqus mass diffusion analysis can be performed by using the general diffusion Equation 5.3 or using an extended Fickian diffusion Equation 5.4 when defining a nonzero pressure stress factor [17].

$$\mathbf{J} = -s\mathbf{D} \cdot \left[\frac{\partial \phi}{\partial \mathbf{x}} + \kappa_s \frac{\partial}{\partial \mathbf{x}} (\ln(\theta - \theta^Z)) + \kappa_p \frac{\partial p}{\partial \mathbf{x}} \right] \quad (5.3)$$

$$\mathbf{J} = -\mathbf{D} \cdot \left(\frac{\partial c}{\partial \mathbf{x}} + s\kappa_p \frac{\partial p}{\partial \mathbf{x}} \right) \quad (5.4)$$

Where

- \mathbf{J} = flux of concentration
- s = solubility
- \mathbf{D} = diffusivity
- ϕ = normalized concentration
- \mathbf{x} = position
- κ_s = temperature gradient factor, "Sorret effect" factor
- θ = temperature
- θ^Z = value of absolute zero temperature scale
- κ_p = pressure stress factor describing diffusion over pressure gradient
- p = equivalent pressure stress
- c = concentration diffusing material

The general diffusion equation as described in Equation 5.3 gives possibilities for defining diffusion driven by pressure gradient, temperature gradient and concentration gradient. However in this case it is assumed pressure and temperature are constant. Not defining these parameters, results in Fick's first law, as described in Equation 5.1 and Equation 5.4 without the κ_p -term.

To develop a concentration gradient in Abaqus, a mass concentration boundary condition is described setting the concentration of the surface to 1, representing submersion. This concentration gradient between outside (1) and inside (0) causes the diffusion to take place. As the concentration is unknown at the beginning, it is assumed to be 0.

Input in the analysis are the diffusion coefficients D in three directions, and the maximum saturation content, or solubility. The diffusion coefficients are extracted with help of experimental results using Equation 5.2, the solubility is determined based on estimations of the asymptotic in diffusion and maximum moisture content of previous research; 0.47%. For steel material it is assumed it does not take up water. Standard linear heat transfer hex (DC3D8) meshing elements are used.

Abaqus determines the sum of the amount of solute in the total volume, SOL , and its progression over time in days. To calculate the moisture content over time Equation 5.5 is applied. The results are then plotted weight increase against square root of time in hours.

$$M_t = SOL/V_{tot} \quad (5.5)$$

Where

- M_t = Moisture content in the volume
- SOL = Amount of solute summed over the total volume
- V_{tot} = Total volume

To compare the experimental values with the FEA, the sum of the error is calculated. First the FEA results are approximated at the timestamps of experimental data by means of local linear regression. Then the absolute difference between the FEA and experimental result at that point in time is determined. The differences over all these points are summed up to form the total error (S).

In all analysis it is assumed that the diffusion is fully caused by Fickian-behaviour. This is however a simplification of the real situation, as explained in Section 5.1.

5.3. Geometries

This section describes the geometries taken into account in this research. It is divided in two groups.

1. Geometries of specimens which were experimentally submerged in 23 °C salt water and used to determine diffusion coefficients using FEA
2. Geometries of specimens which were only evaluated using FEA to model saturation time and profile

For all geometries presented, the coordinate system used as shown in Figure 5.4b represents the x-direction as primary longitudinal, y-axis transverse, and z-direction through-thickness. Next to this, post cured and non-post cured material is evaluated.

1. Experimental

The goal is to use experimental data to determine diffusion coefficients in all directions.

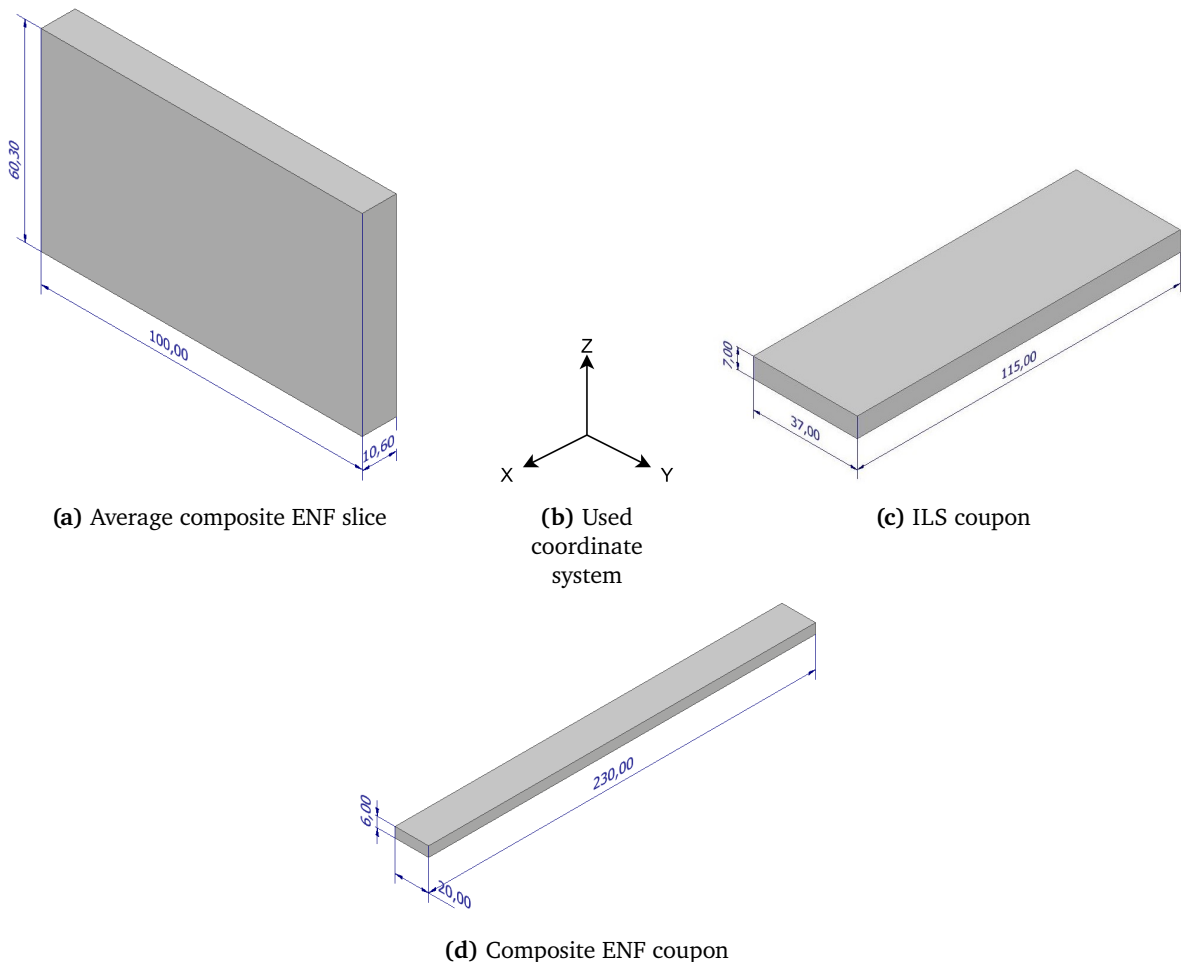


Figure 5.4: Experimental coupon dimensions in mm

- (a) Composite slice of a mechanically tested end notched flexure (ENF) coupon (Figure 5.4a). By minimizing dimension in x-direction, this will be the primary diffusion direction. Measurements can be used to extract D_x . Due to the similarity of composition of material in-plane, it is assumed to be equal to D_y . The material is not post cured. Because the slice is part of a tested coupon, defects in the material, such as micro-cracks, can be present from the start of the submersion experiment
- (b) Composite interlaminar shear (ILS) coupons (Figure 5.4c). After in-plane diffusion coefficients are determined, this geometry is used to determine

through-thickness D_z .

Data is available for post cured and non-post cured specimens.

(c) Composite ENF (Figure 5.4d).

After in-plane diffusion coefficients are determined, this geometry is used to determine through-thickness D_z .

Data is available for post cured and non-post cured specimens.

2. Numerical.

Determine diffusion profile to investigate how moisture progresses at the interface over time.

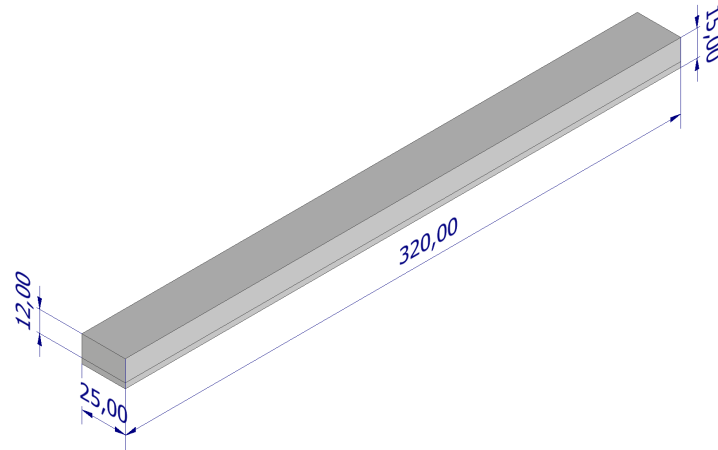


Figure 5.5: Bi-material ENF coupon

(a) Bi-material steel-composite ENF (Figure 5.5)

The goal is to determine the diffusion profile to determine at what stages of ageing water will be present in the steel-composite interface.

The coupons have a 90mm non-adhesive insert on one side, this is however not included in the model due to the unknown exact influence of this on the diffusion

6

Results

This chapter describes the results of the diffusion analysis. Firstly Section 6.1 shows results determining diffusion coefficients in different directions. These determined coefficients are then used in Section 6.2 to predict the saturation profiles of a bi-material coupon over time to determine the presence of water at the interface.

6.1. Experimentally determined diffusion coefficients

6.1.1. In-plane diffusion - ENF slice

First the in-plane diffusion coefficient is determined. As a first estimate of the coefficient, the linear part of the experimental curves are plotted alongside their linear trend lines in Figure 6.1a. The slope of these trend lines is then used together with the geometry of the specific slice to determine the first estimate of the diffusion coefficient using Equation 5.2.

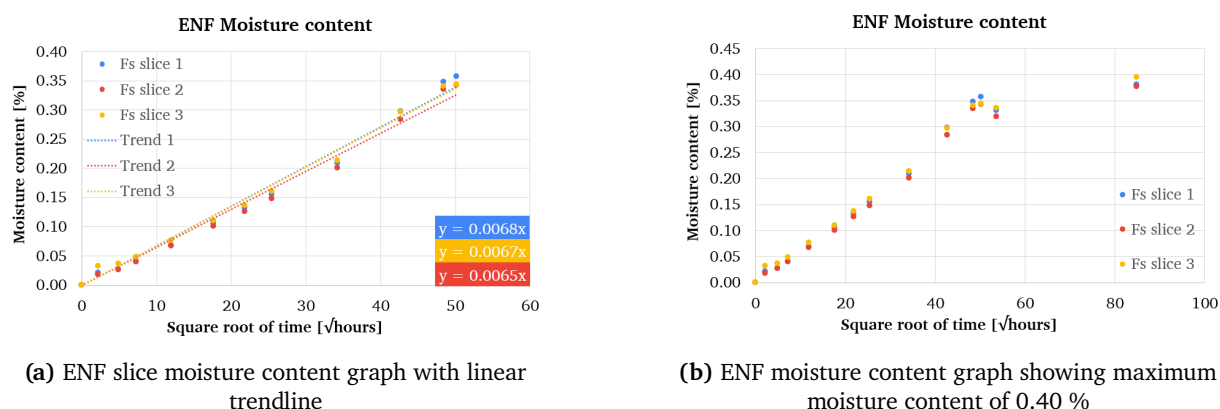


Figure 6.1: ENF slice moisture content graphs

Figure 6.1b shows the linear and non-linear part of the moisture uptake graph of the ENF slices. This figure shows an apparent maximum moisture content of 0.40%, however, previous researched showed a saturation content of 0.47%. As there is no certainty saturation is already reached for the ENF slices, a saturation of 0.47% is assumed. This results in the following estimates for in-plane diffusion coefficient D_x :

Table 6.1: Determined first estimations Diffusion coefficients D_x

Saturation [%]	0.47
	Diffusion coefficient D_x [mm^2/day]
Slice 1	0.103
Slice 2	0.116
Slice 3	0.105

Next to the testing of the ENF coupon, cutting of the slices of the coupon may have caused damages, causing the diffusion coefficient to appear higher. To get a complete image of the diffusion, $D_x = 0.12\text{mm}^2/\text{day}$, $D_x = 0.10\text{mm}^2/\text{day}$, $D_x = 0.08\text{mm}^2/\text{day}$ and $D_x = 0.06\text{mm}^2/\text{day}$ are considered with a saturation of 0.47%. Next to this, D_y is assumed to be equal to D_x , and D_z is assumed to be very small. This is done by taking a very small number for D_z . For all analysis of this geometry a mesh size of 0.5mm is used.

Figure 6.2 shows the different FEA results and an average result of the experiments. Table 6.2 summarizes the sum of the errors (S).

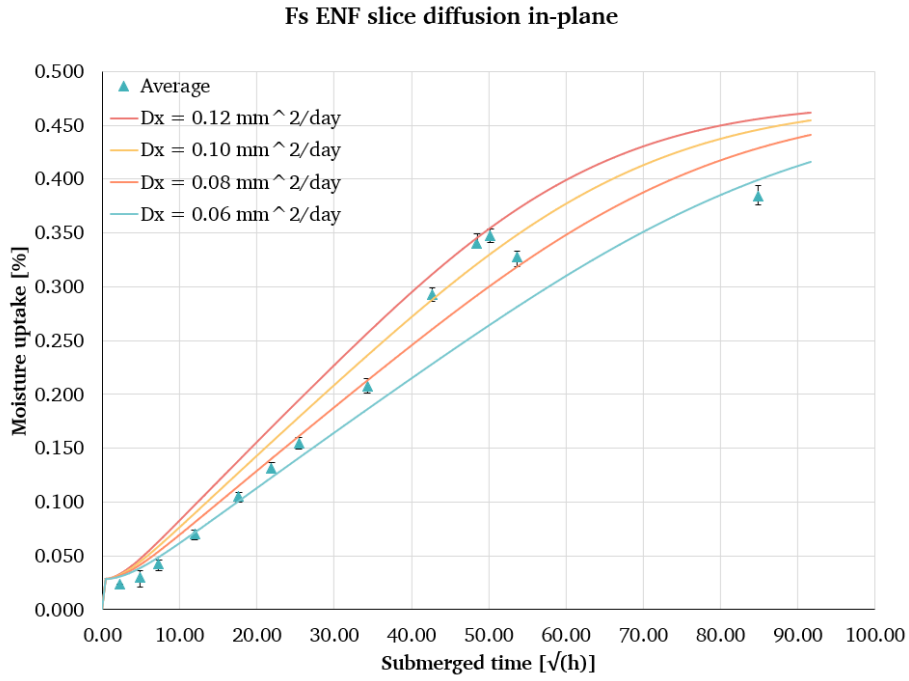


Figure 6.2: FEA results alongside average experimental results ENF slice

Table 6.2: ENF slice sum of errors for different diffusion coefficients

D_x [mm^2/day]	0.06	0.08	0.10	0.12
S [mm^2/day]	0.36	0.25	0.28	0.38

Table 6.2 shows that the error is smallest for $D_x = 0.08\text{mm}^2/\text{day}$, which is thus assumed the in-plane diffusion coefficient

6.1.2. Through-thickness diffusion

Based on the diffusion coefficient in-plane of $0.08\text{mm}^2/\text{day}$, now the through-thickness coefficient D_z will be determined using experimental measurements of ILS coupons and composite ENF coupons.

ILS coupon

Figure 6.3 shows the moisture uptake of post cured and non-post cured ILS coupons with markers. As for the ENF slice, the saturation is set at 0.47% for both post cured and non-post cured material.

The error between FEA results and experimental results are evaluated for both post cured and non-post cured ILS coupons. For the FEA models a mesh size of 0.5mm is used. Figure 6.3 shows the experimental measurements with FEA results for different diffusion coefficients through-thickness.

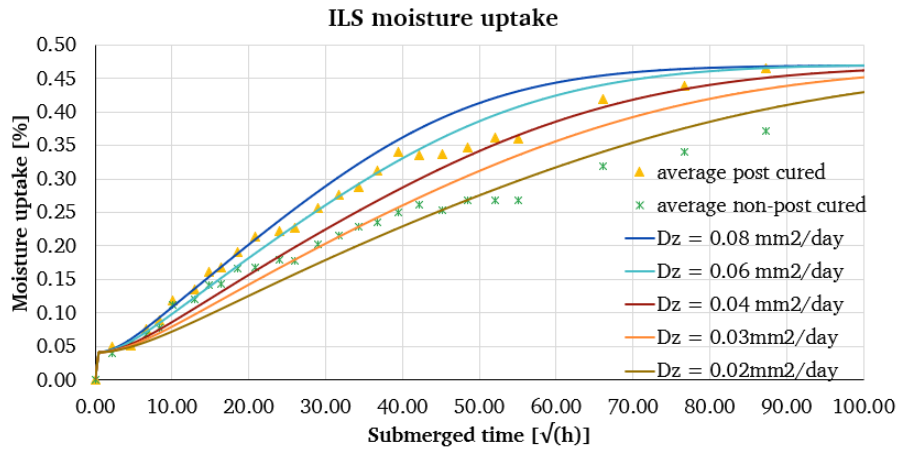


Figure 6.3: FEA results alongside average experimental results post cured ILS coupon

Table 6.3: ILS sum of errors for different diffusion coefficients

	Saturation [%]	D_z [mm^2/day]	0.02	0.03	0.04	0.06	0.08
post cured	0.47	S [mm^2/day]	1.64	1.08	0.65	0.36	0.58
non-post cured	0.47	S [mm^2/day]	0.61	0.62	0.87	1.37	1.84

Figure 6.3 shows for both post cured and non-post cured behaviour it is only possible to find a representative FEA fit for the first phase up until a timestamp of $40\sqrt{\text{hours}}$. When only taking into account this first stage, the sum of total errors is as shown in Table 6.4.

Table 6.4: ILS sum of errors first stage for different diffusion coefficients

	Saturation [%]	D_z [mm^2/day]	0.02	0.03	0.04	0.06	0.08
post cured	0.47	S [mm^2/day]	1.04	0.77	0.54	0.17	0.23
non-post cured	0.47	S [mm^2/day]	0.45	0.22	0.26	0.48	0.78

Composite ENF coupon

Figure 6.4 shows the moisture uptake of post cured composite ENF coupons with markers. The saturation is assumed equal to 0.47%. For the FEA models a mesh size of 0.25mm is used.

Figure 6.4 shows the experimental measurements with FEA results of different diffusion coefficients through-thickness. The sum of the total error is shown in Table 6.5.

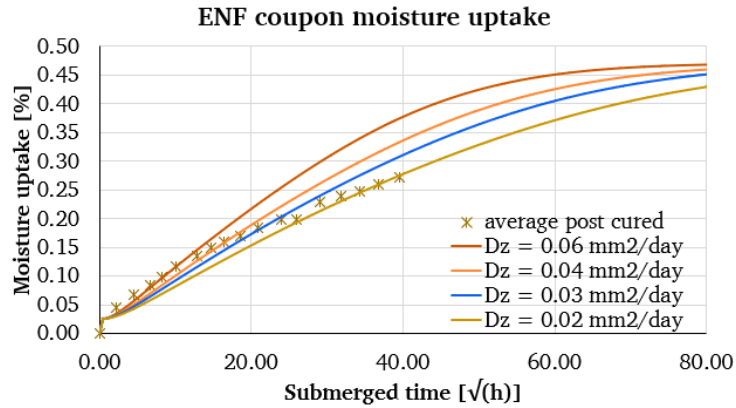


Figure 6.4: FEA results alongside average experimental results composite ENF coupon

Table 6.5: Composite ENF coupon sum of errors for different diffusion coefficients

D_z [mm^2/day]	0.02	0.03	0.04	0.06
S [mm^2/day]	0.32	0.31	0.41	0.72

Conclusion D_z

Table 6.4 and Table 6.5 show the best fit to be with a through-thickness diffusion coefficient $D_z = 0.03 mm^2/day$ for post cured ENF coupons and non-post cured ILS coupons. For post cured ILS coupons, the best fit would be $D_z = 0.06 mm^2/day$.

6.1.3. Summary determined coefficients and saturation

The determined diffusion coefficients can thus be summarised as shown in Table 6.6. A through-thickness diffusion coefficient of $D_z = 0.03 mm^2/day$ is selected. This is done because it provides the best fit for non-post cured ILS coupons, as the ENF slice used for determining D_z was also non-post cured.

Table 6.6: Diffusion coefficients

D_x [mm^2/day]	0.08
D_y [mm^2/day]	0.08
D_z [mm^2/day]	0.03

These values are in in-plane direction higher than previous res. [18] shows $D_{x,y} = 0.06 mm^2/day$ and $D_z = 0.03 mm^2/day$ with a saturation moisture content of 0.47%.

6.2. Prediction diffusion profile bi-material coupons

Using the diffusion coefficients as shown in Table 6.6, a bi-material steel composite 4ENF coupon is modelled (see Figure 5.5). The coupon is only modelled 1/4 to reduce computation time. Figure 6.5 shows in red the sections that are considered. Section A-A a mid-plane section, section B-B a section at the last layer of composite.

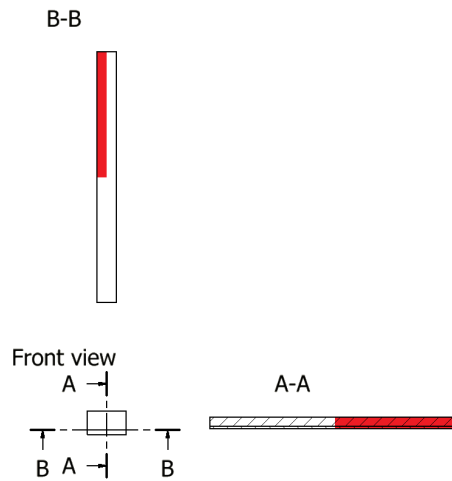


Figure 6.5: Sections used for saturation profiles

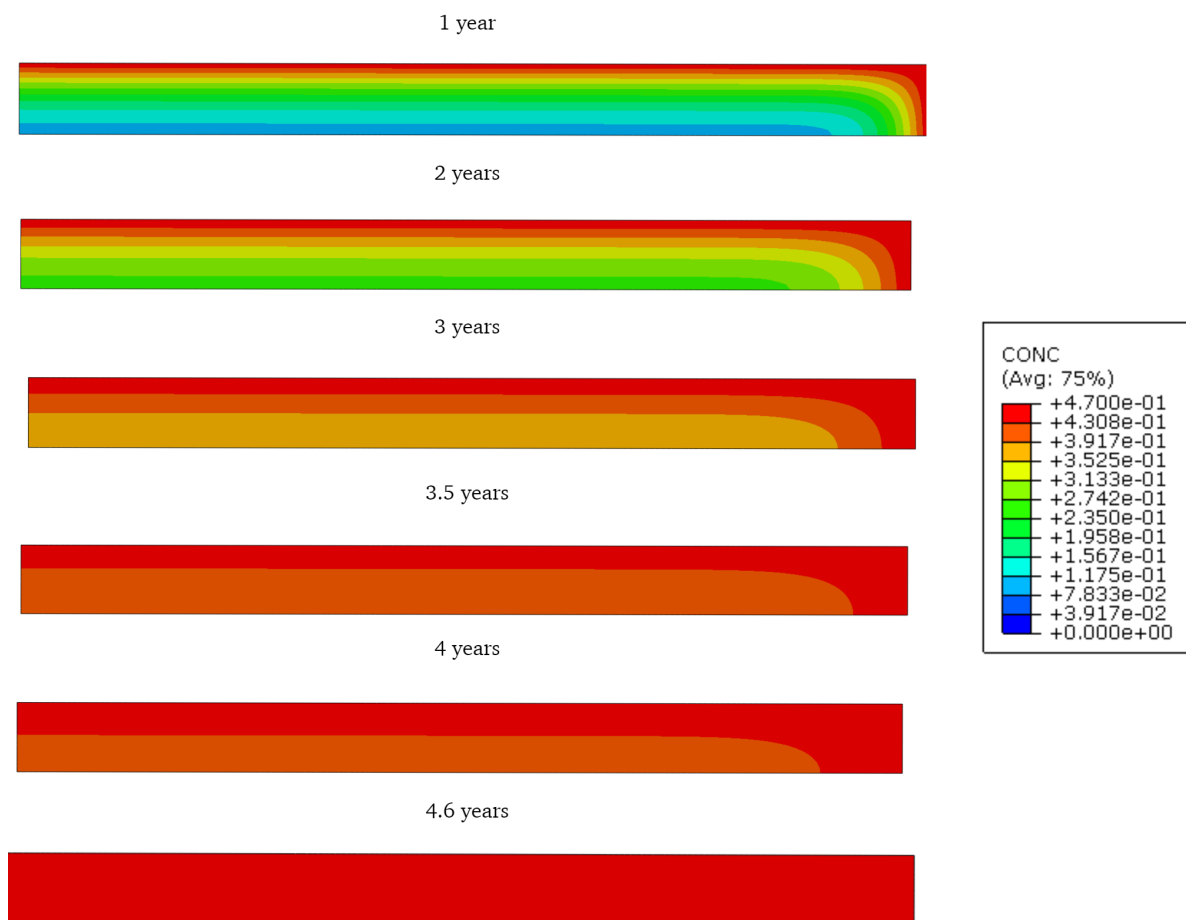


Figure 6.6: Salt water concentration section B-B

The saturation profiles show the concentration of salt water over the cross section. This will show in what period of time moisture will have reached the complete interface when submerging it in salt water.

Figure 6.6 and Figure 6.7 show the concentration in sections A-A and B-B over the years. This show that after 3.5 years the complete specimen has a concentration above 0.40%, 80% of the total saturation content. After 4.6 years, the specimen has reached complete saturation. This is almost half of the predicted 8 years in previous work [18]. In real life this value will be even lower due to the 90 mm non-adhesive insert, which will act as a bridge for water towards the bonded interface.

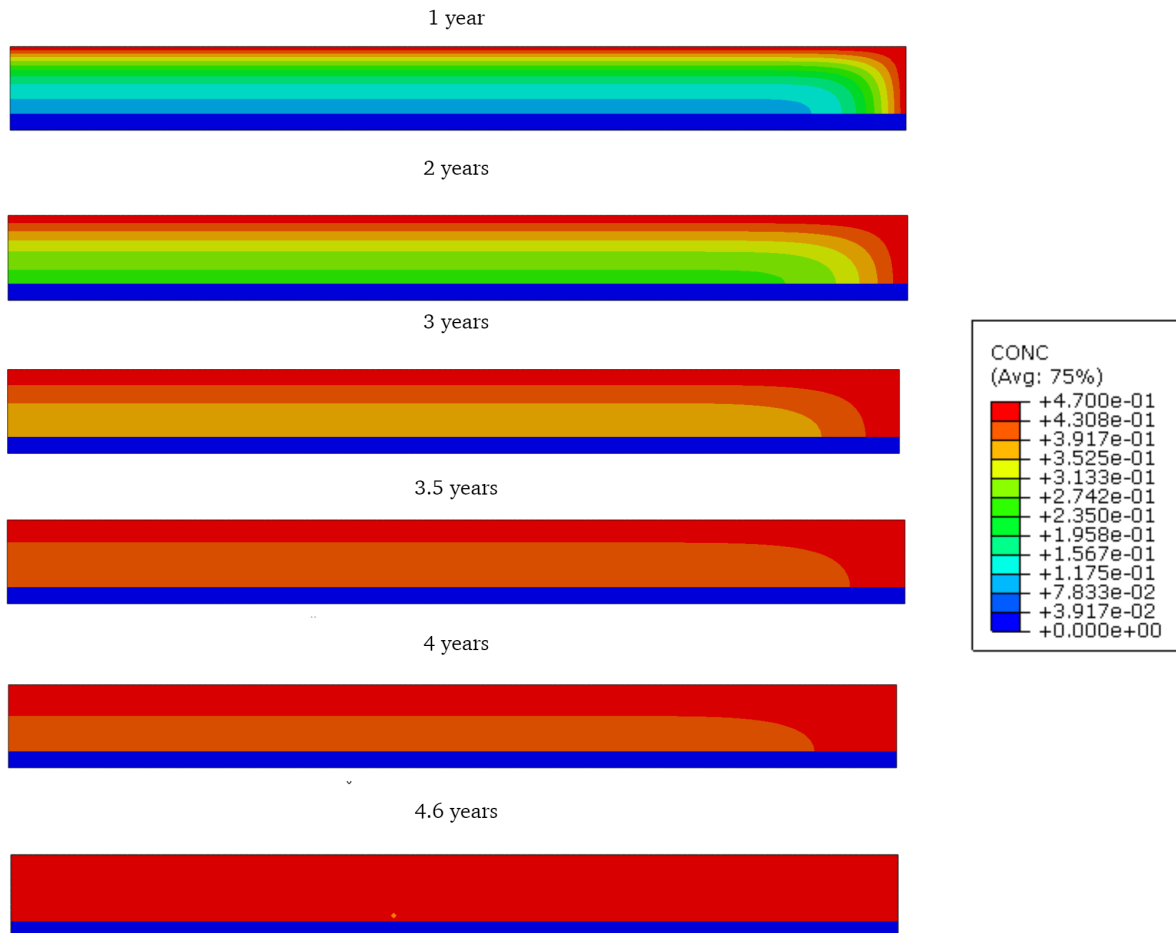


Figure 6.7: Salt water concentration section A-A. Blue bar = steel plate

7

Discussion and conclusion

Chapter 6 shows the results of determining the diffusion coefficients of glassfibre vinyl ester composite in-plane and through-thickness. It was concluded that the in-plane diffusion coefficients are $D_x = 0.08 \text{ mm}^2/\text{day}$ and through-thickness coefficients are $D_z = 0.03 \text{ mm}^2/\text{day}$, as presented in Table 6.6. Next to this, it is concluded that a bi-material ENF coupon would take 4.6 years to completely saturate.

There are however some points to be commented on:

- As mentioned in Section 5.2, the initial moisture content is not taken into account in the models, as it is assumed to be zero for all geometries. However, this has three effects on the results.
 1. By this assumption the saturation content is underestimated, as it is 0.47% on top of the actual initial concentration of the material.
 2. Especially experimental results of non-post cured material will show an underestimation of the moisture content, as before testing they have not been dried back and contain the most moisture when comparing to post cured material.
 3. By this assumption, the gradient between the inside of the material and the exterior is higher, as the gradient is 1. In the real situation this nonzero value would cause the gradient to be smaller, and thus slower diffusion will take place, regardless of the diffusion coefficient.
- The assumption of a saturation content of 0.47% over simplifies the situation. With the experimental results at hand, it is not possible to determine one maximum moisture content for the material, due to the variability in results. Next to non-post cured and post cured specimens having different initial moisture contents, within HLU material there is a scatter in results due to production being prone to human inconsistencies.
- All FEA analysis performed assume pure Fickian behaviour. However, for example for ILS coupons, the experimental results already show there is a possibility degradation is taking place, and multi-staged diffusion is taking place as described in Section 5.1. Figure 7.1 shows the previous presented experimental results, with in black a Fickian curve, and in blue a hypothetical additional moisture uptake curve. To determine if this is taking place, it should be known what the weight loss of specimens is during the experiment. This is however only possible when specimens are dried back.

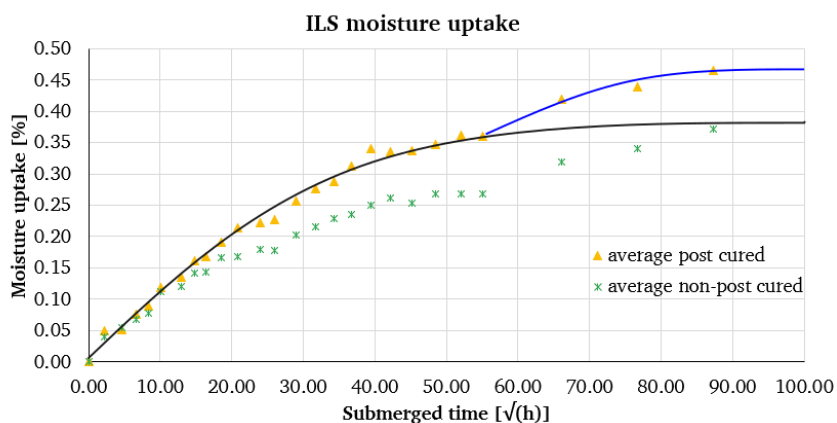


Figure 7.1: Experimental ILS coupon with sketched diffusion curves. Black = Fickian diffusion, blue = additional diffusion due to degradation

Next to that, in theory the diffusivity of the material would be equal for post cured and non-post cured material. However, as seen in Figure 7.1, the non-post cured material after $t = 20\sqrt{\text{hours}}$ gains weight slower, indicating a simultaneous loss of weight. This could be an indication of leeching of non-bounded compounds in the non-post cured specimens due to the not fully completed polymerisation.

- Modelling the saturation of the bi-material coupon without the insert is an overestimation of the time necessary to reach saturation, as the insert will act as a bridge for getting moisture at the interface. This diffusion rate is however impossible to quantify. This because the diffusion along the interface is different from diffusion through the composite due to the different material composition, and metal corrosion dominates weight change of the bi-material coupons, making experimental weight change unsuitable for tracking behaviour. 4.6 years until saturation is thus a value that should be used with caution.

To improve upon the models, a few suggestions are made for further research:

- Before starting diffusion experiments, and during experiments, periodically take specimens out and dry them back to determine if weight loss has taken place. This will be an indication of degradation, helping guide what stages of diffusion are still Fickian. These results then can be used to more accurately determine maximum moisture content of the material, which will greatly increase accuracy of models.
- For determining pure Fickian diffusion coefficients, conduct experiments with in-plane diffusion dominant, and with through-thickness diffusion dominant with post cured specimens. Due to the increased polymerisation in post cured material, the result will be closer to Fickian, and will guide in not underestimating diffusion rates in the material.
- Based on experimental data perform sensitivity study of minor changes of saturation and of diffusion coefficients. This will help guide what issues are at hand during the life time of the structure, and which are purely hypothetical.

References

- [1] P. He et al. “Feasability of wrapped FRP circular hollow section joints”. In: *Proceedings of the 17th International Symposium on Tubular Structures* (2020). DOI: 10.3850/978-981-11-0745-0_043-cd.
- [2] European committee for standardization. *TS 19101: 2021 Design of fibre-polymer composite structures*. Tech. rep. TB, 2023.
- [3] Technische Universität Dresden. *eLamX²*. 2023. URL: https://tu-dresden.de/ing/maschinenwesen/ilr/lft/elamx2/elamx?set_language=en.
- [4] ASTM International. *ASTM D696-16 Standard Test Method for Coefficient of Linear Thermal Expansion of Plastics Between -30°C and 30°C with a Vitreous Silica Dilatometer*. Tech. rep. 2018.
- [5] Linseis. *DIL L75 PT Horizontal, Research Dual- and Differential Dilatometer series*. 2024. URL: <https://www.linseis.com/en/products/dilatometer/dil-l75-pt-horizontal/>.
- [6] ASTM International. *ASTM E228-22 Standard Test Method for Linear Thermal Expansion of Solid Materials with a Push-Rod Dilatometer*. Tech. rep. 2018.
- [7] ASTM International. *Standard Test Method for Linear Thermal Expansion of Rigid Solids with Interferometry*. Tech. rep. 2017. DOI: 10.1520/E0289-17.
- [8] Perkin Elmer. *TMA 4000*. 2024. URL: <https://www.perkinelmer.com/uk/product/tma-4000-lab-system-100-230v-l8040000>.
- [9] International Organization for Standardization. *ISO 11359-2 Plastics — Thermomechanical analysis (TMA) — Part 2: Determination of coefficient of linear thermal expansion and glass transition temperature*. Tech. rep. 2021.
- [10] Struers. *TEGRAMIN, An all-round system for process standardization and high-quality specimen preparation*. 2024. URL: <https://www.struers.com/en/Products/Grinding-and-Polishing/Grinding-and-polishing-equipment/Tegramin#references>.
- [11] A. Paul et al. *Thermodynamics, Diffusion and the Kirkendall Effect in Solids*. Springer International Publishing Switzerland, 2014. DOI: 10.1007/978-3-319-07461-0_3.
- [12] Chi-Hung Shen et al. “Moisture Absorption and Desorption of Composite Materials”. In: *Journal of Composite Materials* 10 (1976), pp. 2–20. DOI: 10.1177/002199837601000101.
- [13] Carol L. Schutte. “Environmental durability of glass-fiber composites”. In: *Materials Science and Engineering: R: Reports* 13.7 (1994), pp. 265–323. DOI: [https://doi.org/10.1016/0927-796X\(94\)90002-7](https://doi.org/10.1016/0927-796X(94)90002-7). URL: <https://www.sciencedirect.com/science/article/pii/0927796X94900027>.
- [14] Weiping He et al. “Experimental Investigation on Hygroscopic Aging of Glass Fiber Reinforced Vinylester Resin Composites”. In: *Polymers* 14 (Sept. 2022), p. 3828. DOI: 10.3390/polym14183828.
- [15] J.C. Arnold et al. “An assessment of methods to determine the directional moisture diffusion coefficients of composite materials”. In: *Composites Part A: Applied Science and Manufacturing* 55 (2013), pp. 120–128. DOI: <https://doi.org/10.1016/j.compositesa.2013.08.012>. URL: <https://www.sciencedirect.com/science/article/pii/S1359835X13002364>.
- [16] Xu Jiang et al. “Moisture diffusion in glass-fiber-reinforced polymer composite bridge under hot/wet environment”. In: *Composites Part B: Engineering* 45.1 (2013), pp. 407–416. DOI: <https://doi.org/10.1016/j.compositesb.2012.04.067>. URL: <https://www.sciencedirect.com/science/article/pii/S135983681200306X>.
- [17] MIT. *Mass diffusion analysis*. 2024. URL: <https://abaqus-docs.mit.edu/2017/English/SIMACAEANLRefMap/simaanl-c-massdiffusion.htm>.

-
- [18] P. Karatsi. *Durability of composite to steel bi-material joints*. 2023.